Journal of Medicinal Chemistry

Article

pubs.acs.org/jmc

Free-Wilson and Structural Approaches to Co-optimizing Human and Rodent Isoform Potency for 11β-Hydroxysteroid Dehydrogenase Type 1 (11β-HSD1) Inhibitors

Frederick W. Goldberg,* Andrew G. Leach, James S. Scott, Wendy L. Snelson, Sam D. Groombridge, Craig S. Donald, Stuart N. L. Bennett, Cristian Bodin, Pablo Morentin Gutierrez, and Amy C. Gyte

AstraZeneca, Mereside, Alderley Park, Macclesfield, SK10 4TG, United Kingdom

Supporting Information

ABSTRACT: 11β-Hydroxysteroid dehydrogenase 1 (11β-HSD1) has been a target of intensive research efforts across the pharmaceutical industry, due to its potential for the treatment of type II diabetes and other elements of the metabolic syndrome. To demonstrate the value of 11β-HSD1 in preclinical models, we required inhibitors with good potency against both human and rodent isoforms. Herein, we describe our efforts to understand how to co-optimize human and murine potency within the (5-hydroxy-2-adamantyl)-pyrimidine-5-carboxamide series. Two approaches are described—a data-driven (Free-Wilson) analysis and a structure-based design approach. The conclusions from these approaches were used to inform an efficient campaign to design compounds with consistently good human/murine potency within a log$D_{7.4}$ range of 1−3. Compounds **20** and **26** demonstrated good rodent PK, which allowed us to demonstrate a PK/PD relationship in rat and mouse. We then evaluated **26** against glycemic and body weight end points in murine disease models, where it demonstrated glucose and body weight efficacy at 300 mg/kg/day but only body weight efficacy at 50 mg/kg/day, despite providing >90% target engagement in the liver.

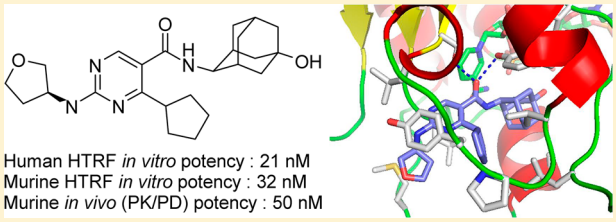

INTRODUCTION

11β-Hydroxysteroid dehydrogenase 1 (11β-HSD1) has been a target of intensive research efforts across the pharmaceutical industry,[1,2] due to its potential for the treatment of type II diabetes and other elements of the metabolic syndrome.[3,4] Demonstrating preclinical in vivo efficacy has been a challenge, however, because of the nature of the in vivo models and the difficulty in identifying inhibitors with good potency against both human and rodent isoforms, as we found in our discovery of 2-[(3*S*)-1-[5-(cyclohexylcarbamoyl)-6-propylsulfanylpyridin-2-yl]-3-piperidyl]acetic acid (AZD4017).[5] In a previous communication,[6] we described our efforts to identify 11β-HSD1 inhibitors with improved PK; key to that success was switching the core from pyridine to pyrimidine. Pyrimidines such as **1** (Figure 1) demonstrated good potency against both human and murine isoforms, but it was noticed that further co-optimizing the potency against both isoforms was challenging as the human/murine SAR was orthogonal in some cases. In this paper, we describe our efforts to demonstrate preclinical target engagement and identify compounds for murine efficacy models, by co-optimizing human and rodent potency of neutral compounds within the (5-hydroxy-2-adamantyl)-pyrimidine-5-carboxamide series. Two approaches are described—a data driven (Free-Wilson) analysis and a structural approach.

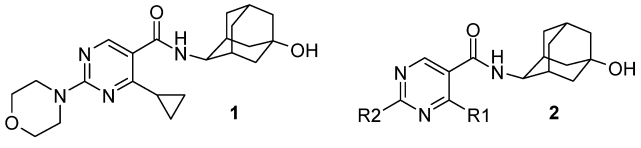

Human 11β-HSD IC_{50} 102 nM

Murine 11β-HSD IC_{50} 95 nM

Figure 1.

RESULTS AND DISCUSSION

A Free-Wilson approach[7] assumes that the SAR between substructures is additive and thus potency and properties of new compounds, comprised of known substituents, may be predicted using the observed contributions of the substituents on a specific core. It can be a powerful method in the context of a mature research program, where data exist on a wide variety of substructures and the goal is to efficiently and rapidly optimize parameters such as potency and lipophilicity. We felt that the (5-hydroxy-2-adamantyl)-pyrimidine-5-carboxamide scaffold **2** (Figure 1) was suitable for this approach as the core had given good PK properties (**1** gave 100% oral bioavailability in rat and dog)[6] and the R1 and R2 groups are assumed to be conformationally independent. We therefore analyzed the data we had to predict effects on murine and

Received: September 12, 2012
Published: November 16, 2012

dx.doi.org/10.1021/jm3013163 | *J. Med. Chem.* 2012, 55, 10652−10661

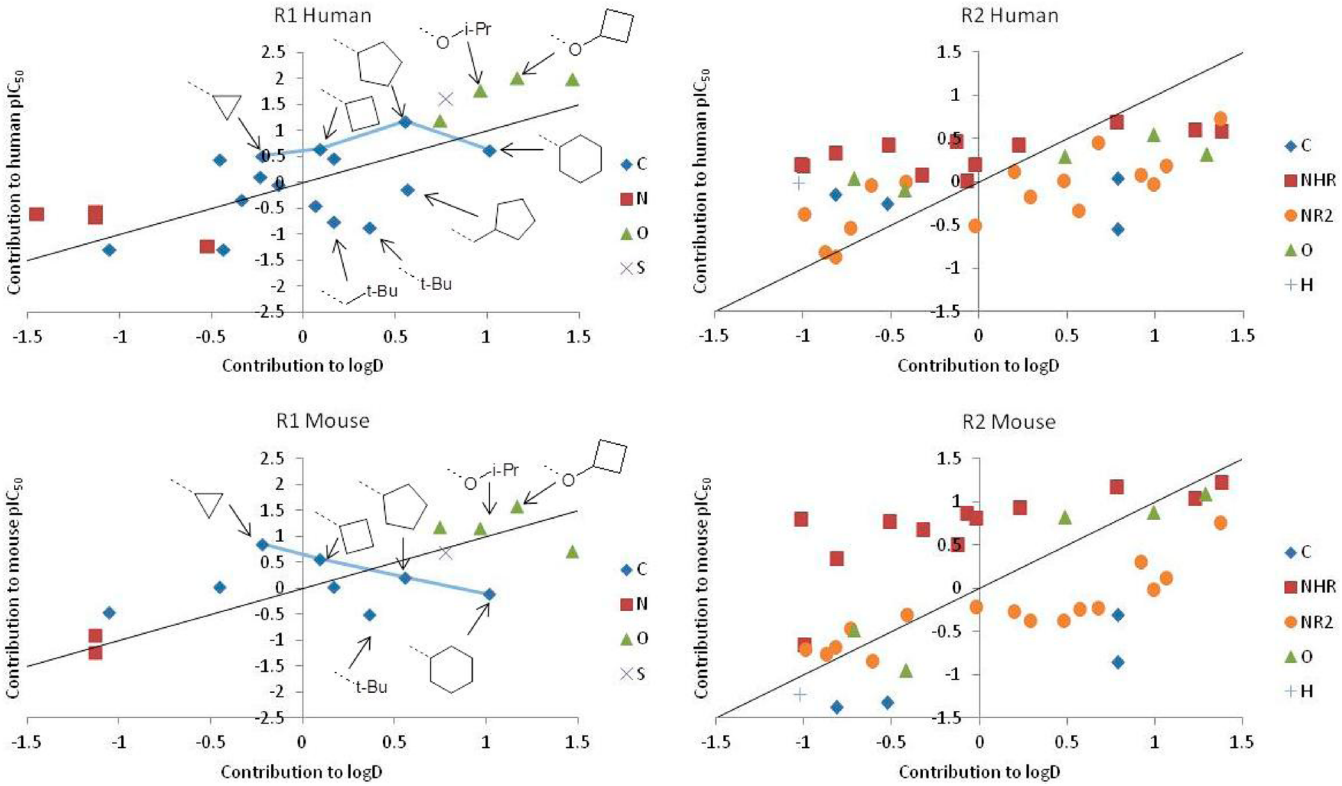

Figure 2. Free-Wilson model contributions for groups at R1 and R2 toward human and murine in vitro pIC_{50} vs equivalent group contribution toward $logD_{7.4}$. The 1:1 line is shown (black), and groups above this line contribute to improvements in LLE. The blue line (R1) indicates the effect of increasing size of cycloalkyl groups.

human potency of R1 and R2 for this scaffold. This analysis was then used to analyze global trends (e.g., with size and polarity) and to evaluate new combinations of R1 and R2, as well as new isosteric groups, that might give high potency against both isoforms when applied to the (5-hydroxy-2-adamantyl)-pyrimidine-5-carboxamide scaffold. We aimed to do this without increasing logD, that is, to improve ligand lipophilicity efficiency (LLE, defined in this article as pIC_{50}-$logD_{7.4}$).[8]

To demonstrate that SAR is additive in a Free-Wilson type analysis, Oyarzabal et al.[9] have recommended studying the R^2 values for predictions made on a test set after model building on a training set and recommend that additive models should produce R_{test}^2 values greater than 0.6. In our case, most models for both human and murine potency (only using in-range values) achieve this and so are shown to be additive. The mean value of R_{test}^2 for human potency is 0.72 and for murine potency is 0.79 with standard deviations of 0.10 and 0.12, respectively. The standard error in each mean is 0.03, demonstrating that at 95% confidence, the underlying population mean is greater than 0.6, thus supporting the conclusion that group contributions from R1 and R2 are additive. More detailed parameters are provided in the Supporting Information.

With confidence that the SAR was additive, we built Free-Wilson models for each species covering the full set of compounds to assess the contribution that the different groups at R1 and R2 make to human/murine in vitro potency and $logD_{7.4}$. The coefficients computed for the various groups within the Free-Wilson model are plotted in Figure 2, where the contributions of R1 and R2 groups toward human and murine pIC_{50} are plotted against contributions toward $logD_{7.4}$ as estimated by a Free-Wilson model for that property. For R1 in human, the majority of substituents sit on or above a 1:1 line for pIC_{50}:logD; that is, potency is driven by lipophilicity. The groups that sit significantly below the 1:1 line are structural features that are apparently not well tolerated, for example, in this plot, ^{t}Bu, $CH_2{}^t$Bu, and CH_2-cyclopentyl (*c*-Pn) for human, suggesting that these groups are too big. Murine potency shows a similar trend for lipophilicity driving potency, and again, large lipophilic groups such as cyclohexyl sit off the 1:1 murine pIC_{50}:logD line. Our conclusion from this analysis is that R1 is a difficult position to improve LLE as there is an excellent correlation between potency and logD for the preferred groups, so limited effort should be expanded on optimizing the R1 position. We choose a narrow range of lipophilic ether/alkyl R1 groups, controlling the size to ensure a good balance between human and murine potency but focused elsewhere on the scaffold to use polar groups to improve LLE and physicochemical properties.

For R2, the correlations between potency and lipophilicity are less clear, reflecting more subtle SAR where specific polar interactions can be picked up. This data set largely reflects amine SAR since most compounds tested were 2-amino-pyrimidines (see the Supporting Information for the data set used and resulting Free-Wilson contributions). Within that restriction, it can be seen that having a donor is apparently important for murine potency but not essential for human potency. This general trend is exemplified by the distribution of points for secondary (NHR) and tertiary (NR2) nitrogen substituents (Figure 2, R2 mouse), and so we concluded that secondary groups at R2 should allow us to achieve good levels of human and murine potency. There is also a slight trend

dx.doi.org/10.1021/jm3013163 | J. Med. Chem. 2012, 55, 10652−10661

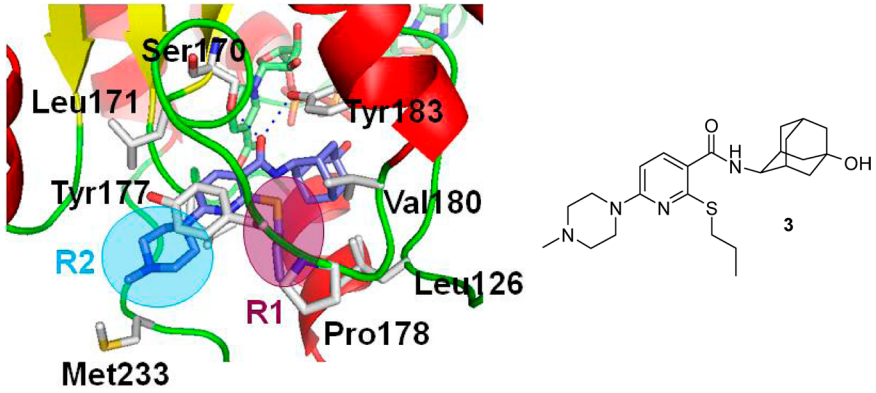

Figure 3. Binding site of the complex of **3** with the human isoform of 11β-HSD (4bb6), in which the side chains of all residues within 4 Å of the ligand are shown. The region that the R1 and R2 groups on the pyrimidine are expected to occupy is indicated in maroon and light blue ovals, respectively. NADP is shown in the background with green-colored carbon atoms, and the hydrogen bonds between Ser170 and Tyr183 are indicated with blue dashed lines.

toward bigger, more lipophilic groups increasing both human and murine potency, although the trend is less pronounced than for R1. The R2 group apparently offers a wider scope for different size and lipophilicity and the opportunity to incorporate polar groups to control logD and properties.

In tandem with the Free-Wilson approach detailed above, the wealth of structural information available both internally and externally was examined. At that time, there was no available structure of a pyrimidine amide bound to 11β-HSD1, but a structure of a related pyridine had been obtained internally (PDB code: 4bb6). Along with many of the publicly available structures of complexes with 11β-HSD1, this suggested that the binding mode is dominated by correct positioning of the adamantyl amide (or equivalent donor) group.[10] We made the assumption that although the specific SAR may differ between the series, the broad positions in space of the groups around the pyrimidine core would be similar to those around the pyridine core of compound **3** shown in Figure 3.

The enzyme consists to a great extent of fairly rigid helices and sheets, but the site immediately surrounding the binding site is dominated by flexible loops. This suggests that the binding site is likely to be mobile. It should be noted that there are two molecules in the asymmetric repeat, and the conformation of the ligand and receptor is similar in both, and so only one is shown here. It is a subject of debate whether the dimer is relevant to the in vivo situation or just an artifact of the crystallographic experiment and in vitro assays.[11−14] In Figure 3, the binding site is shown together with the NADP cofactor. The principal interaction is likely related to the mechanism of action of the enzyme and consists of two hydrogen bonds to the amide carbonyl formed by Ser170 and Tyr183. This carbonyl group is also positioned in close proximity to the C4 position of the nicotinamide segment of NADP from where hydride delivery takes place during the reduction of cortisone to cortisol. The adamantyl group is buried in the deeper part of the pocket, and it is likely that this region is occupied by a hydrophobic section of the steroid during the normal enzymatic process. This is consistent with the adamantyl amide being a mimic of the substrate and/or transition state and therefore making a significant contribution to the affinity of the ligand for the enzyme.

The structure shown in Figure 3 demonstrates the regions into which the R1 (maroon oval) and R2 (light blue oval) would be expected to bind if the pyrimidine series were to bind in an analogous fashion to the pyridine of **3**. This provides some interesting rationalization of the SAR that was suggested by the Free-Wilson analysis. The R1 group is in a lipophilic pocket lined by the Leu126, Tyr177, Pro178, and Val180 residues. The region occupied by R2 is bounded by the lipophilic regions of Leu171, Leu217, and Met233 but also by the side chain of Tyr177, which has its hydroxyl group oriented toward R2. This is consistent with the SAR above in which R1 tends to be lipophilic to enhance human potency and R2 has more varied SAR in which hydrogen-bonding groups may be tolerated. Presumably, groups that can interact favorably with either the hydroxyl or the electron-rich aromatic side chain of Tyr177 might enhance potency while reducing lipophilicity.

The contrast between the structures of human and murine 11β-HSD1 is illustrated in Figure 4. As a murine structure was not available to us internally, the murine structure is taken from the complex with *n*-octane reported by Zhang et al. (PDB code: 1y5m).[15] The murine structure was overlaid on that of the complex of the human form with **3** using the protein superposition function in Maestro.[16]

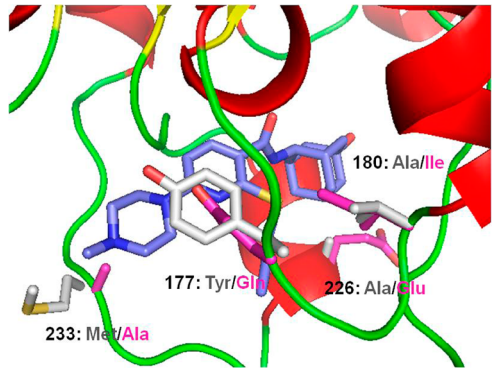

Figure 4. Complex of **3** with murine 11β-HSD1 generated by overlay of the complex shown in Figure 3 and the complex of murine 11β-HSD1 with *n*-octane (1y5m). In pink are the murine residues that were within 4 Å of the ligand in the human complex and are different in humans; residue labels are shown in gray for humans and pink for murine.

It is interesting to note that the lipophilic pocket into which R1 protrudes has a key residue in human (Ala180) that is larger in murine (Ile180). This reduces the size of the pocket slightly

dx.doi.org/10.1021/jm3013163 | J. Med. Chem. 2012, 55, 10652−10661

Scheme 1. Synthetic Route for R1 = Alkyl[a]

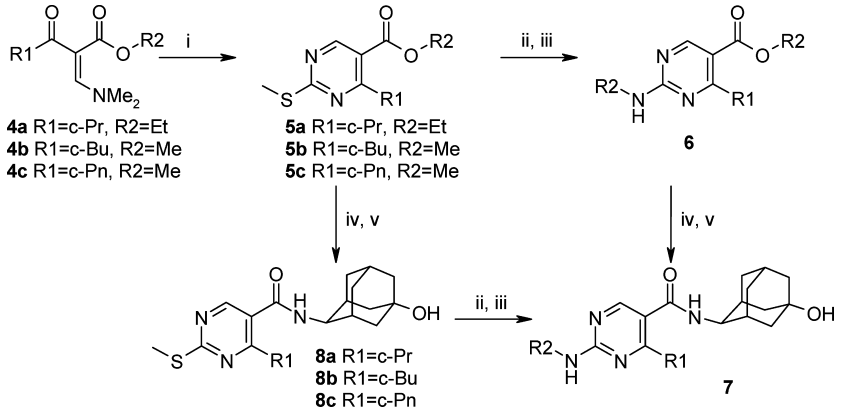

[a]Reagents and conditions: (i) 2-Methyl-2-thiopseudourea sulfate, NaOAc, DMF, 44−80%. (ii) Oxone, MeCN, H_2O or *m*CPBA, DCM, 82−94%. (iii) $R2NH_2$, *i*-Pr_2NEt, THF, 23−100%. (iv) 2 M aqueous NaOH, MeOH, 64−95%. (v) HATU, *trans*-4-aminoadamantan-1-ol·HCl, *i*-PrNEt, DMF, 58−88%.

Scheme 2. Synthetic Route for R1 = Ether[a]

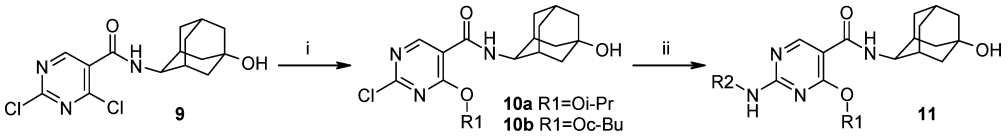

[a]Reagents and conditions: (i) R1ONa, THF or R1OH, 51−91%. (ii) $R2NH_2$, *i*-Pr_2Net, *n*-PrCN or THF, 23−39%.

and also enables smaller groups [such as cyclopropyl (*c*-Pr), see Figure 2] to make hydrophobic contacts in the murine isoform form that they are not able to make in human; hence, small groups at R1 are better tolerated in murine. Similarly, whereas *c*-Pn is a good group for human potency and presumably makes good contacts with Ala180, in murine, the group may clash with the larger Ile180. The Free-Wilson and protein−ligand complex both suggest that large lipophilic groups at R1 are preferred for human potency, but smaller lipophilic groups are preferred for murine potency.

By contrast, the region that R2 protrudes into is dominated by the change from Tyr177 (human) to Gln177 (murine). This large change in the size and physical properties of the residue is likely a key cause of the spread about the line seen in the Free-Wilson analysis shown in Figure 2. It is striking that the flexible Gln side chain that can interact with donors and acceptors is consistent with a favoring of NH-alkyl for murine activity in the group contributions identified in the Free-Wilson analysis. It could also be argued that the Gln carbonyl is a stronger acceptor than the Tyr phenol (so stronger preference for a donor on the ligand for murine potency), although rationalizing that a priori would have been difficult without the Free-Wilson analysis. The groups shown in Figure 2 that are able to contribute to both human and murine potency are presumably able to form good interactions with both Gln and Tyr in this position. The position is relatively open to solvent in both isoforms and so larger groups ought to be tolerated in both species.

Using the conclusions from the Free-Wilson and structural analyses, our strategy relied upon using a limited set of five cycloalkyl/ether R1 groups (lipophilic groups without additional polarity) that were well tolerated for both isoforms according to the Free-Wilson analysis and a more expansive set of 20 secondary amine R2 groups with additional polarity to control logD and explore optimal placement of donors and acceptors. We selected compounds with a predicted $logD_{7.4}$ of 1−3 to increase the chances of obtaining favorable PK properties.[17,18] The R1 groups chosen were *c*-Pr, cyclobutyl (*c*-Bu), *c*-Pn, cyclobutyloxy, and isopropoxy, which were all on the pIC_{50}/logD leading edge of the Free-Wilson plot (i.e., predicted to give high LLE).

Synthetic routes were developed that enabled us to readily vary the R1 and R2 groups. Thus, for targets with an alkyl R1 group, enamine **4** (synthesized from corresponding ketoester) was converted to 2-methylthiopyrimidine **5** with 2-methyl-2-thiopseudourea sulfate (Scheme 1). The thioether was then oxidized to the sulfone with oxone and displaced with an amine to give **6**. Intermediate **6** was then converted to the target compound **7** via saponification and subsequent 2-(3*H*-[1,2,3]-triazolo[4,5-*b*]pyridin-3-yl)-1,1,3,3-tetramethylisouronium hexafluorophosphate(V) (HATU)-mediated amide coupling with *trans*-4-aminoadamantan-1-ol. This route was generally reliable across a range of functionality and reproducible on scale-up. However, an alternative route was also used to convert **5** to the corresponding amide **8** before addition of the R2 amine. Although this route was more capricious, it allowed us to vary R2 as the last step.

For targets with an ether R1 group, the synthesis started with addition of *trans*-4-aminoadamantan-1-ol to 2,4-dichloropyrimidine-5-carbonyl chloride to give amide **9** (Scheme 2). The addition of alkoxides to **9** occurred selectively in the C4 position to give **10**, and subsequent addition of the relevant R2 primary amine provided us with the desired product **11**. Again, this route allowed us to vary the R2 group at the last step, which suited the optimization strategy of fixing R1 as a small number of lipophilic ethers but varying the R2 amine more extensively to pick up polar interactions.

dx.doi.org/10.1021/jm3013163 | *J. Med. Chem.* 2012, 55, 10652−10661

Table 1. Effect of R1 and R2 Groups on Human/Murine Potency and $logD_{7.4}$

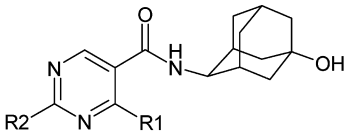

R2 =

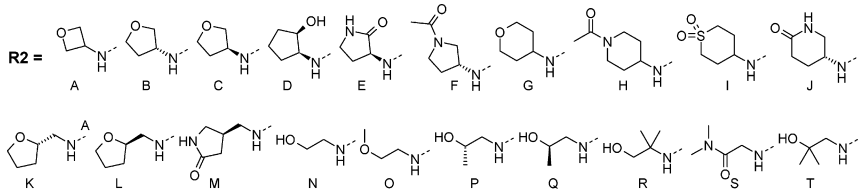

ex.	R1	R2	IC_{50} (nM)[a] human	IC_{50} (nM)[a] murine	$logD_{7.4}$	rat F (%)[b]
12	*c*-Pr	A	74	38	1.1	
13	*c*-Pr	B	30	32	1.6	
14	*c*-Pr	C	36	30	1.7	73
15	*c*-Pr	G	53	22	1.8	53
16	*c*-Pr	R	94	20	1.8	
17	*c*-Pr	T	108	31	1.5	
18	*c*-Bu	B	23	37	2	99
19	*c*-Bu	C	31	42	1.8	82
20	*c*-Bu	G	28	27	2.1	100
21	*c*-Bu	I	54	53	1.1	
22	*c*-Bu	N	31	168	1.3	
23	*c*-Bu	T	46	47	1.8	86
24	*c*-Pn	A	9	66	2.1	
25	*c*-Pn	B	21	25	2.4	63
26	*c*-Pn	C	21	32	2.4	61
27	*c*-Pn	D	29	36	2.7	17
28	*c*-Pn	E	94	55	0.9	
29	*c*-Pn	F	25	50	1.8	18
30	*c*-Pn	G	23	38	2.6	
31	*c*-Pn	H	38	84	1.9	46
32	*c*-Pn	I	16	64	1.6	
33	*c*-Pn	J	27	133	1.6	
34	*c*-Pn	K	27	25	2.7	
35	*c*-Pn	L	22	42	2.8	
36	*c*-Pn	M	34	85	1.4	9
37	*c*-Pn	N	12	179	1.8	
38	*c*-Pn	O	15	73	2.4	
39	*c*-Pn	P	22	42	2	
40	*c*-Pn	Q	26	67	2	68
41	*c*-Pn	R	30	32	2.5	
42	*c*-Pn	S	45	163	1.4	
43	*c*-Pn	T	19	48	2.3	33
44	O*i*-Pr	A	13	53	2.2	57
45	O*i*-Pr	B	11	21	2.7	62
46	O*i*-Pr	C	20	35	2.5	83
47	O*c*-Bu	A	12	33	2.6	19
48	O*c*-Bu	B	12	16	2.9	99
49	O*c*-Bu	C	20	22	2.8	99
50	O*c*-Bu	G	30	19	3.2	83
51	O*c*-Bu	I	48	31	2.1	
52	O*c*-Bu	N	14	31	2.5	51
53	O*c*-Bu	R	30	20	3.1	161

[a]Human and murine potency as measured by the geometric mean of (at least) two independent IC_{50} measurements in a homogeneous time-resolved fluorescence (HTRF) assay; see the Supporting Information for assay details. The standard error of the mean (SEM) is not shown as both human and murine HTRF assays were found to be highly reproducible on repeat testing (pIC_{50} SEM typically <0.1). [b]Oral bioavailability observed in male Han Wistar rats at low dose (po 7.4−14.7 μmol/kg suspension, iv 2.3−5.6 μmol/kg solution); drug concentrations measured in whole blood.

dx.doi.org/10.1021/jm3013163 | *J. Med. Chem.* 2012, 55, 10652−10661

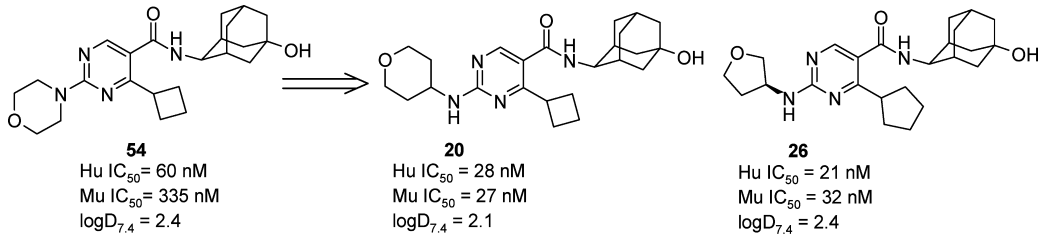

Figure 5. Effect on potency of switching R2 from tertiary to secondary amines.

Rather than synthesizing the whole R1xR2 matrix, we chose to enumerate all 20 R2 amines (Table 1) with R1 = *c*-Pn and select a smaller selection of key R2 amines for the other R1 groups to give the 42 compounds given in Table 1. *c*-Pn was chosen for the full enumeration as it gives higher human potency than *c*-Pr and *c*-Bu (see Figure 2), albeit at the cost of reduced murine potency, and at the time, we had less data on the PK properties of O-linked R1 groups so that these groups were perceived as being higher risk. The design of the R2 amines in part depended on exact groups identified by the Free-Wilson analysis as being good for human and murine potency. Examples of this approach include 1,1-dioxothian-4-amine (**21**, **32**, and **52**, Table 1) and oxetan-3-amine (**12**, **24**, **44**, and **47**). However, we also used the conclusions from the Free-Wilson analysis, in conjunction with the structural analysis, to design new (i.e., not in the Free-Wilson data set) isosteric groups at R2 with suitable placement of acceptors to explore SAR and give favorable predicted properties. Examples of these isosteric groups are tetrahydrofuran-3-amine (**13**/**14**, **18**/**19**, **25**/**26**, **45**/**46**, and **48**/**49** for *R*/*S* enantiomers) and 2-aminocyclopentanol (**27**). The data in Table 1 demonstrate that we succeeded in synthesizing compounds with consistently high human and murine potency. Remarkably, all 42 compounds synthesized in this campaign had an IC_{50} < 180 nM in both human and murine assays, and typical IC_{50} values are in the 10−100 nM range. The SAR is relatively flat, as commented upon in the Free-Wilson analysis. An interesting example of this flat SAR is the similar potencies given by *R*/*S* enantiomers of tetrahydrofuran-3-amine, where all human and murine potencies are within 2-fold between the enantiomers. We concluded that human and murine potencies within this series are apparently not particularly sensitive to the exact placement of the acceptor at R2. Measured $logD_{7.4}$ was generally in the desired 1−3 range, with measured logD values being very accurately predicted (±0.2) by our AstraZeneca calculated logD model $AZlogD_{7.4}$.[18] This model is built on measured $logD_{7.4}$ data on compounds in the AstraZeneca corporate collection. The notable exceptions were all compounds where R1 = O*c*-Bu (compounds **47**−**53**), where the measured logD was ∼0.5 units higher than predicted; for example, **50** and **53** (the most lipophilic compounds in this set) both gave a predicted $AZlogD_{7.4}$ of 2.6, but measured $logD_{7.4}$ values were higher at 3.2 and 3.1, respectively (publically available model $ACDlogD_{7.4}$ v12 also underpredicts **50** and **53** as being 2.2 and 2.1, respectively). Rat bioavailability of these compounds was generally good as shown in Table 1 with 18/23 compounds profiled showing rat *F* > 40% (for more detailed in vivo PK parameters on selected compounds, see Table 3). This campaign thus very efficiently generated a large number of suitable compounds to profile in vivo. In particular, compounds **13**, **20**, **26**, **46**, **48**, and **49** all have excellent human and murine potency with good oral exposure in Han Wistar rats. We selected compounds **20** and **26** to progress into more advanced in vivo studies due to them having a shorter half-life than **13**, **46**, **48**, and **49**. This was a desirable feature preclinically as it allowed us to examine the effects of continuous cover versus episodic dosing to target the cortisol diurnal peak,[20] to address our concerns that target engagement may reduce on chronic dosing with continuous cover. Data to support this hypothesis will be published shortly.

Key to the success was the switch to secondary amines at R2. As can be seen in Figure 5, switching the morpholine at R2 in compound **54** (disclosed in a previous communication[6]) to tetrahydropyran-4-amine increases murine potency and thus gives compound **20**, which combines good human and murine potency at moderate logD. Also shown in Figure 5 is isomeric **26**, which also demonstrated good human/murine potency at moderate logD.

Compounds **20** and **26** were profiled further in vitro to establish that they are potent inhibitors of human 11*β*-HSD1 (Table 2) and selective against related targets. Thus, **20** and **26**

Table 2. Human in Vitro Potency of 20 and 26 against 11*β*-HSD1 and Related Targets

	11*β*-HSD1	11*β*-HSD1	11*β*-HSD2	17*β*-HSD1	17*β*-HSD3
ex.	IC_{50} (HTRF) (nm)	IC_{50} (HPLC) (nm)	IC_{50} (HTRF) (*μ*M)	IC_{50} (HPLC) (*μ*M)	inh (HPLC)
20	28	14	>30	>35	4% at 10 *μ*M
26	21	1.6	>30	>100	7% at 10 *μ*M

gave HTRF potencies of 21 and 28 nM, respectively, and HPLC potencies of 2 and 14 nM, respectively (see the Supporting Information for assay details). The HPLC assay is a low-throughput assay that accounts for tight binding and thus should give a more accurate in vitro potency than the HTRF assay. Both compounds were inactive against 11*β*-HSD2, which is important as 11*β*-HSD2 is believed to be responsible for the reverse reaction in vivo (11*β*-HSD1 primarily converts cortisone to cortisol, whereas 11*β*-HSD2 primarily converts cortisol to cortisone), and has been associated with increased risk of hypertension.[19] Both compounds were also inactive against two 17*β*-hydroxysteroid dehydrogenases tested (17*β*-HSD1 and 17*β*-HSD3).

We were also able to obtain a crystal structure of **26** (Figure 6). The structure of **26** in complex with 11*β*-HSD1 (PDB code: 4bb5) crystallizes such that there are four protein−ligand complexes in the asymmetric unit. The protein conformation is broadly the same in all four complexes including in the vicinity of the binding site. The exception is the solvent-exposed side chain of Met233, which is solved with four different conformations; as might be expected for what seems to be a dynamic side chain, the electron density does not strongly

dx.doi.org/10.1021/jm3013163 | J. Med. Chem. 2012, 55, 10652−10661

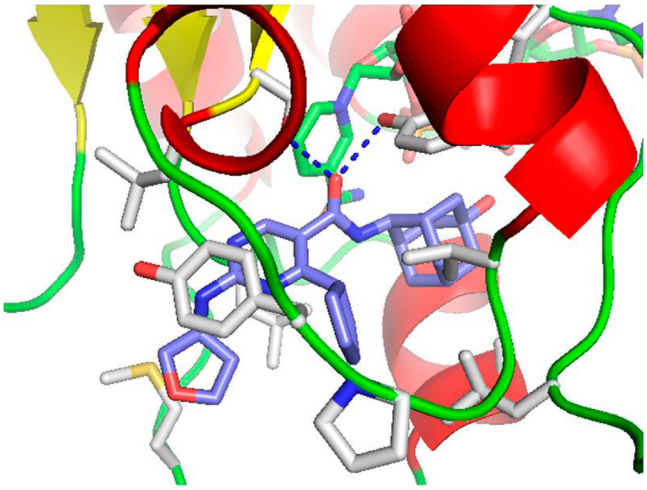

Figure 6. Crystal structure of **26** bound to the human isoform of 11β-HSD1 (4bb5).

support any particular conformation. As can be seen by comparing Figure 6 to Figure 3, the core of the ligand and the binding site side chains are essentially in the same positions, supporting our previous approach of using the pyridine structure for compound **3** to design changes to the pyrimidine series.

PK Properties and PK/PD Relationship of 20 and 26. Compounds **20** and **26** were profiled in vivo and demonstrated suitable PK properties in mouse and rat at low dose (Table 3) to proceed to PK/PD studies. Good oral exposure was seen in mouse and rat. The clearance in both species for both compounds was relatively low considering the high plasma protein binding (PPB) free levels seen in vitro (i.e., low unbound clearance). The relatively short half-lives observed were advantageous as commented previously, to investigate the effects of continuous cover versus episodic dosing. We also profiled both compounds in dog to determine the suitability of **20** and **26** as potential clinical candidates. Human PPB was low for both compounds (52% free for **20** and 38% free for **26**) and both compounds were stable to human hepatocytes (CL_{int} < 2 μL/min/10^6).

Compound **20** was dosed orally to C57 male mice and Han Wistar male rats to study its capacity to inhibit 11β-HSD1 activity in adipose tissue, and a similar study was performed with **26** in C57 male mice. Dose–response experimental designs were carried out with doses of **20** up to 5 (mouse) and 60 mg/kg (rat) and with doses of **26** up to 35 mg/kg (mouse). Figure 7 shows the PK/PD relationships between the ex vivo activity of the 11β-HSD1 enzyme in epididymal adipose tissue (measured as the conversion of ^{3}H-cortisone to ^{3}H-cortisol) and drug concentrations of **20** and **26**. A direct response PK/PD model (E_{max} sigmoidal model) was used to successfully fit the PK/PD data showing, in each case, a clear correlation between free compound levels in plasma and inhibition in the activity of 11β-HSD1 in adipose tissue (see the Supporting Information for ex vivo assay details and model-fitting parameters).

In each case, the in vivo IC_{50} in the ex vivo adipose assay is in very good agreement with the in vitro potency (values shown in Table 4), suggesting that systemic exposure, defined as free compound concentration in plasma, is a good surrogate of drug concentration at the target in adipose tissue. The absolute in vitro and in vivo potencies are within 3-fold of each other in each case, suggesting only 1-fold free cover of the in vitro IC_{50} is required to demonstrate target engagement in vivo.

We then evaluated **26** against glycemic and body weight efficacy end points in a murine disease model. Although **26** did demonstrate a significant lowering in fasting plasma glucose and body weight efficacy (Figure 8), this was achieved at a high dose (300 mg/kg/day) where unbound plasma concentrations of compound **26** were approximately 80 times the in vitro (HTRF) IC_{50}. A separate study (unpublished results), in collaboration with Anne White's group at the University of Manchester, has shown that compound **26** gave body weight and glucose efficacy at high dose (300 mg/kg/day). However, lowering the dose to 50 mg/kg/day resulted only in body weight efficacy without a significant lowering of fasting glucose despite providing >90% target engagement in liver and ~30 fold free cover over the in vitro IC_{50} in plasma.

CONCLUSIONS

Free-Wilson and structure-based design approaches were taken to co-optimizing potency against human and murine isoforms of 11β-HSD1, within the (5-hydroxy-2-adamantyl)-pyrimidine-5-carboxamide series. The conclusions from both approaches helped to inform an efficient design based on picking a limited number of lipophilic, low molecular weight R1 groups with a more expansive exploration of R2 secondary amines. This work identified a number of neutral compounds that were potent against both isoforms in the desired $logD_{7.4}$ range (1–3) and led to the identification of compounds **20** and **26**, which have good PK in mouse and rat, and successfully demonstrated murine/rat target engagement in ex vivo assays. We then evaluated **26** against body weight and glycemic end points in

Table 3. PK Properties of 20 and 26

ex.	species	iv/po dose (μmol/kg)	iv CL (mL/min/kg)	iv $t_{1/2}$ (h)	iv V_{ss} (L/kg)	po AUC (μM h)	F (%)	PPB % free	Hep CL_{int}[d] (μL/min/10^6)
20	mouse[a]	4.7/11.7	42	0.4	1.1	2.7	57	>50	3.6
	rat[b]	4.7/11.7	32	0.6	0.9	10.4	100	55	<2
	dog[c] m	1.0/1.2	19	0.8	1.1	0.38	34	>66	<2
	dog[c] f	1.0/1.2	29	0.7	1.6	0.16	23	>66	<2
26	mouse[a]	4.7/11.7	57	0.7	2.4	1.5	34	30	9.1
	rat[b]	4.7/7.0	9	2.4	1.0	5.6	61	35	<2
	dog[c] m	0.6/1.2	17	0.6	0.7	0.19	15	38	6.7
	dog[c] f	0.6/1.2	14	0.6	0.6	0.42	30	38	6.7

[a]Dosed (suspension for po and solution for iv) to male mice; drug concentrations measured in whole blood. [b]Dosed (suspension for po and solution for iv) to male Han Wistar rats; drug concentrations measured in whole blood. [c]Dosed as solution to Beagles (m = male, and f = female); drug concentrations measured in plasma. [d]In vitro median CL_{int} observed with hepatocytes from the appropriate species.

dx.doi.org/10.1021/jm3013163 | J. Med. Chem. 2012, 55, 10652–10661

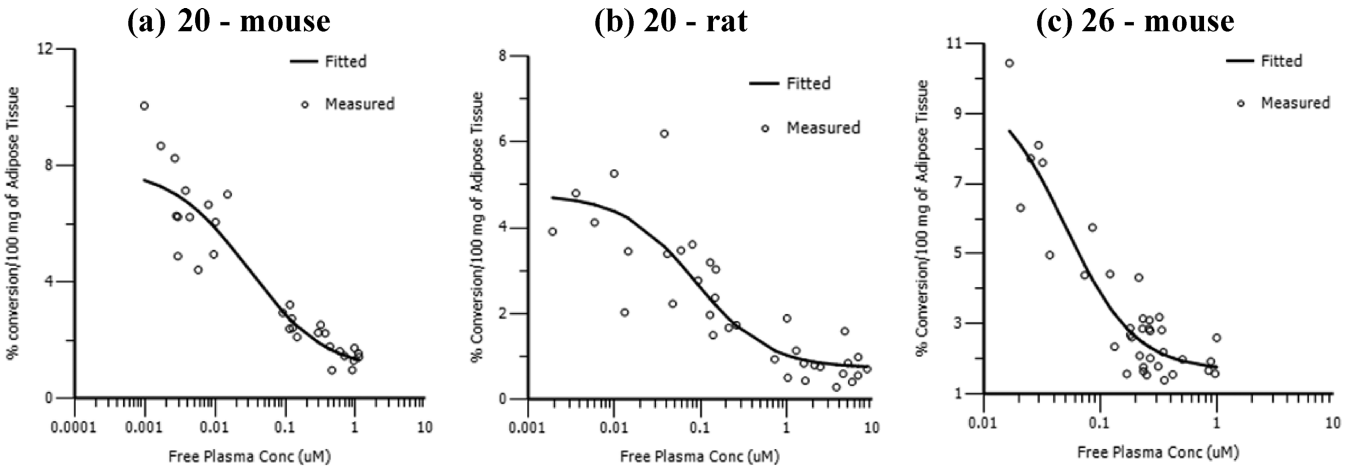

Figure 7. PK/PD relationship between the ex vivo activity of the 11β-HSD1 enzyme in epididymal adipose tissue and the drug concentrations of (a) **20** in male C57 mice, (b) **20** in male Han Wistar rats, and (c) **26** in male C57 mice.

Table 4. Comparison of in Vitro Potency to Ex Vivo Potency from the in Vivo PK/PD Study

ex.	species	in vitro IC_{50} (μM)[a]	in vivo IC_{50} (μM)[b]
20	mouse	0.027	0.030
	rat	0.271	0.087
26	mouse	0.032	0.050

[a]Measured in HTRF assay (see the Supporting Information for details). [b]Measured ex vivo, using epididymal adipose tissue samples from the in vivo PK/PD study as the conversion of ^{3}H-cortisone to ^{3}H-cortisol.

murine disease models, where it demonstrated glucose and body weight efficacy at 300 mg/kg/day but only body weight efficacy at 50 mg/kg/day, despite providing >90% target engagement in the liver at both doses.

EXPERIMENTAL SECTION

All solvents and chemicals used were reagent grade. Flash column chromatography was carried out using prepacked silica cartridges from Redisep, Biotage, or Crawford and eluted using an Isco Companion system. Purity and characterization of compounds were established by a combination of LC-MS and NMR analytical techniques and was >95% for all compounds. ^{1}H NMR were recorded on a Bruker Avance DPX400 (400 MHz) and were determined in DMSO-d_6, unless stated otherwise. ^{13}C NMR spectra were recorded at 101 or 175 MHz. Chemical shifts are reported in ppm relative to tetramethylsilane (TMS) (0 ppm) or solvent peaks as the internal reference. All MS data were obtained using electrospray. Merck precoated thin-layer chromatography (TLC) plates (silica gel 60 F254, 0.25 mm, art. 5715) were used for TLC analysis. Preparative HPLC was performed on C18 reversed-phase silica on a Waters or Phenomenex preparative reversed-phase column using decreasingly polar mixtures of water (containing 1% formic acid or 1% aqueous NH_4OH) and MeCN. All reactions were performed under nitrogen unless otherwise stated.

Methyl 2-(Cyclobutanecarbonyl)-3-(dimethylamino)acrylate (4b). DMF dimethyl acetal (5.62 mL, 42.3 mmol) was added in one portion to methyl 3-cyclobutyl-3-oxopropanoate (5.5 g, 35.2 mmol) in 1,4-dioxane (50 mL) at rt. The resulting solution was stirred at 100 °C for 4 h. The reaction mixture was concentrated, and the resulting crude product was purified by flash column chromatography (FCC), eluting with 50−80% EtOAc/isohexane, to afford the title compound (4.60 g, 62%). ^{1}H NMR ($CDCl_3$): 1.72−1.82 (1H, m), 1.85−1.97 (1H, m), 2.06−2.13 (2H, m), 2.18−2.29 (2H, m), 3.02 (6H, s), 3.68−3.75 (1H, m), 3.73 (3H, s), 7.62 (1H, s). m/z $[M + Na]^+$ = 234. HPLC t_R = 1.42 min.

Methyl 4-Cyclobutyl-2-(methylthio)pyrimidine-5-carboxylate (5b). 2-Methyl-2-thiopseudourea sulfate (1.93 g, 13.9 mmol) was added to methyl 2-(cyclobutanecarbonyl)-3-(dimethylamino)-acrylate **4b** (2.6 g, 12.3 mmol) and sodium acetate (4.24 g, 51.7 mmol) in DMF (10 mL) at rt. The resulting solution was stirred at 80 °C for 2 h. Water was added to the cooled solution. The reaction mixture was diluted with EtOAc and washed with water. The organic layer was dried over $MgSO_4$, filtered, and evaporated to afford crude product. The crude product was purified by FCC, elution gradient 5−30% EtOAc in isohexane to afford the title compound (1.30 g, 44%) as a white solid. ^{1}H NMR ($CDCl_3$): 1.86−1.94 (1H, m), 2.00−2.10 (1H, m), 2.26−2.35 (2H, m), 2.41−2.51 (2H, m), 2.65 (3H, s), 3.90 (3H, s), 4.35 (1H, qn), 8.86 (1H, s). m/z MH^+ = 239. HPLC t_R = 2.75 min.

4-Cyclobutyl-2-(methylthio)pyrimidine-5-carboxylic Acid. A solution of $LiOH.H_2O$ (0.458 g, 10.9 mmol) in water (8 mL) was added to a stirred solution of methyl 4-cyclobutyl-2-(methylthio)-

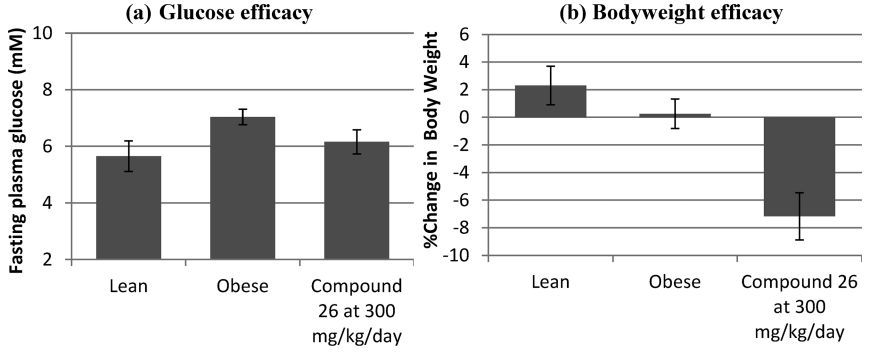

Figure 8. Fasting plasma glucose and body weight changes of lean mice, obese mice, and obese mice treated with compound **26**.

dx.doi.org/10.1021/jm3013163 | J. Med. Chem. 2012, 55, 10652−10661

pyrimidine-5-carboxylate **5b** (1.3 g, 5.46 mmol) in THF (16 mL) at rt. The resulting mixture was stirred at rt for 24 h. The THF was evaporated, and the resulting aqueous layer was washed with EtOAc, then was acidified with 1 M aqueous citric acid, and extracted with EtOAc. The organic layer was washed with saturated brine, dried over $MgSO_4$, filtered, and evaporated to afford the title compound (1.10 g, 90%) as a white solid. ^{1}H NMR ($CDCl_3$): 1.87−1.96 (1H, m), 2.02−2.13 (1H, m), 2.31−2.39 (2H, m), 2.44−2.54 (2H, m), 2.67 (3H, s), 4.42 (1H, qn), 9.00 (1H, s), no CO_2H peak observed. *m*/*z* MH^+ = 225. HPLC t_R = 0.82 min.

4-Cyclobutyl-*N*-((2*s*,5*r*)-5-hydroxy-2-adamantyl)-2-methylsulfanylpyrimidine-5-carboxamide (8b). *i*-Pr_2NEt (3.39 mL, 19.6 mmol) was added to 4-cyclobutyl-2-(methylthio)pyrimidine-5-carboxylic acid (1.1 g, 4.90 mmol), *trans*-4-aminoadamantan-1-ol hydrochloride (1.10 g, 5.40 mmol), and HATU (2.24 g, 5.89 mmol) in DMF (20 mL) at rt. The reaction mixture was stirred at rt for 24 h, then was evaporated to dryness, taken up in EtOAc. and washed sequentially with water and saturated brine. The organic layer was dried over $MgSO_4$, filtered, and evaporated to afford crude product. The crude product was purified by FCC, eluting with 0−6% MeOH in DCM, to afford the title compound (1.50 g, 82%) as a white solid. ^{1}H NMR ($CDCl_3$): 1.55−1.62 (2H, m), 1.66−1.71 (2H, m), 1.78−1.85 (5H, m), 1.91−1.97 (3H, m), 2.00−2.08 (1H, m), 2.15−2.19 (1H, m), 2.23−2.32 (4H, m), 2.43−2.52 (2H, m), 2.62 (3H, s), 3.92−4.00 (1H, m), 4.17−4.22 (1H, m), 5.90 (1H, d), 8.41 (1H, s). *m*/*z* MH^+ = 374. HPLC t_R = 2.00 min.

4-Cyclobutyl-*N*-((2*s*,5*r*)-5-hydroxy-2-adamantyl)-2-methylsulfonylpyrimidine-5-carboxamide. 3-Chloroperoxybenzoic acid (70%) (0.937 g, 3.80 mmol) was added in one portion to 4-cyclobutyl-*N*-(5-hydroxy-2-adamantyl)-2-methylsulfanylpyrimidine-5-carboxamide **8b** (0.71 g, 1.90 mmol) in DCM (35 mL) at 0 °C. The reaction mixture was allowed to warm to rt, was stirred at rt for 24 h, and then was taken up in DCM. The organic layer was washed sequentially with saturated aqueous $NaHCO_3$, 2 M aqueous NaOH, and saturated brine, dried over $MgSO_4$, filtered, and evaporated to afford crude product. The crude product was purified by FCC, eluting with 0−6% MeOH in DCM, to afford the title compound (0.560 g, 73%) as a white solid. ^{1}H NMR ($CDCl_3$): 1.44 (1H, s), 1.58−1.65 (2H, m), 1.74−1.87 (6H, m), 1.93−1.98 (3H, m), 2.05−2.15 (1H, m), 2.18−2.30 (3H, m), 2.32−2.39 (2H, m), 2.43−2.55 (2H, m), 3.34 (3H, s), 4.00−4.09 (1H, m), 4.21−4.28 (1H, m), 6.42 (1H, d), 8.71 (1H, s). *m*/*z* MH^+ = 406. HPLC t_R = 1.59 min.

4-Cyclobutyl-*N*-[(2*r*,5*s*)-5-hydroxyadamantan-2-yl]-2-(tetrahydro-2*H*-pyran-4-ylamino)pyrimidine-5-carboxamide (20). 4-Cyclobutyl-*N*-((2*s*,5*r*)-5-hydroxy-2-adamantyl)-2-methylsulfonylpyrimidine-5-carboxamide (270 mg, 0.67 mmol) and tetrahydro-2*H*-pyran-4-amine (269 mg, 2.66 mmol) were dissolved in THF (4 mL) and sealed into a microwave tube. The reaction was heated to 150 °C for 1 h and cooled to rt. The reaction mixture was diluted with DCM and stirred with saturated aqueous $NaHCO_3$ before passing through a phase separation cartridge. The organic layer was evaporated to afford crude product, which was purified by preparative HPLC to afford the title compound (169 mg, 60%) as a white solid. ^{1}H NMR: 1.31 (2H, d), 1.48−1.58 (2H, m), 1.61 (4H, m), 1.68−2.01 (11H, m), 2.10 (2H, q), 2.23−2.32 (2H, m), 3.35−3.41 (2H, m), 3.86 (4H, m), 3.98 (1H, m), 4.37 (1H, s), 7.31 (1H, d), 7.92 (1H, d), 8.13 (1H, s). *m*/*z* MH^+ = 427. HPLC t_R = 1.67 min.

Methyl 2-(Cyclopentanecarbonyl)-3-(dimethylamino)-acrylate (4c). DMF dimethyl acetal (3.28 mL, 24.7 mmol) was added in one portion to methyl 3-cyclopentyl-3-oxopropanoate (3.50 g, 20.6 mmol) in 1,4-dioxane (40 mL) at rt. The resulting solution was stirred at 100 °C for 4 h. The reaction mixture was evaporated to afford crude product. The crude product was purified by FCC, eluting with 50−80% EtOAc in isohexane, to afford the title compound (4.50 g, 97%) as a yellow oil. ^{1}H NMR: 1.45−1.73 (8H, m), 2.81−2.86 (1H, m), 2.95 (6H, s), 3.62 (3H, s), 7.57 (1H, s). *m*/*z* MH^+ = 226. HPLC t_R= 1.66 min.

Methyl 4-Cyclopentyl-2-(methylthio)pyrimidine-5-carboxylate (5c). 2-Methyl-2-thiopseudourea hemisulfate (84 g, 607 mmol) was added in one portion to methyl 2-(cyclopentanecarbonyl)-3-(dimethylamino)acrylate **4c** (114 g, 506 mmol) and NaOAc (166 g, 2024 mmol) in DMF (500 mL). The reaction mixture was stirred at 80 °C for 2 h, then at rt for 14 h, and then was partially evaporated. The reaction mixture was diluted with EtOAc and washed with water. The organic layer was dried over $MgSO_4$, filtered, and evaporated to afford crude product. The crude product was purified by FCC, eluting with 0−20% EtOAc in isohexane to afford the title compound (76 g, 60%) as a cream solid. ^{1}H NMR ($CDCl_3$): 1.67−1.72 (2H, m), 1.79−1.92 (4H, m), 1.99−2.05 (2H, m), 2.58 (3H, s), 3.91 (3H, s), 3.99−4.09 (1H, m), 8.85 (1H, s). *m*/*z* MH^+ = 253. HPLC t_R = 3.04 min.

Methyl 4-Cyclopentyl-2-(methylsulfonyl)pyrimidine-5-carboxylate. Oxone (48.7 g, 79.3 mmol) was added to methyl 4-cyclopentyl-2-(methylthio)pyrimidine-5-carboxylate 5c (10 g, 39.6 mmol) in acetonitrile (75 mL) and water (75 mL). The reaction mixture was stirred at rt for 16 h and then was concentrated, saturated aqueous $NaHCO_3$ was added dropwise, and the mixture was extracted with DCM. The organic layers were combined, dried over $MgSO_4$, filtered, and concentrated to afford the title compound (9.70 g, 86%). ^{1}H NMR: 1.67 (2H, m), 1.81 (4H, m), 2.02 (2H, m), 3.43 (3H, s), 3.92 (1H, m), 3.94 (3H, s), 9.24 (1H, s). *m*/*z* MH^+ = 285. HPLC t_R = 2.08 min.

(*S*)-Methyl 4-cyclopentyl-2-(tetrahydrofuran-3-ylamino)-pyrimidine-5-carboxylate. *i*-Pr_2NEt (4.91 mL, 28.1 mmol) was added to methyl 4-cyclopentyl-2-(methylsulfonyl)pyrimidine-5-carboxylate (4 g, 14.1 mmol) and (*S*)-tetrahydrofuran-3-amine hydrochloride (2.61 g, 21.1 mmol) in THF (50 mL). The resulting solution was stirred at rt for 16 h. The reaction mixture was concentrated, taken up in DCM, and washed sequentially with water and saturated aqueous $NaHCO_3$. The organic layer was dried over $MgSO_4$, filtered, and evaporated to afford the title compound (2.55 g, 62%). ^{1}H NMR: 1.67 (2H, m), 1.82 (4H, m), 1.97 (3H, m), 2.20 (1H, m), 3.61 (1H, m), 3.77 (1H, q), 3.82 (3H, s), 3.97 (3H, m), 4.46 (1H, m), 8.08 (1H, d), 8.72 (1H, s). *m*/*z* MH^+ = 292. HPLC t_R = 2.30 min.

(*S*)-4-Cyclopentyl-2-(tetrahydrofuran-3-ylamino)pyrimidine-5-carboxylic Acid. Two molar aqueous NaOH (8.72 mL, 17.4 mmol) was added to a solution of (*S*)-methyl 4-cyclopentyl-2-(tetrahydrofuran-3-ylamino)pyrimidine-5-carboxylate (2.54 g, 8.72 mmol) in methanol (40 mL) at rt. The resulting mixture was stirred at 40 °C for 16 h, and then, the reaction was stirred at 55 °C for 4 h. The reaction mixture was concentrated, taken up in water, and washed with EtOAc. The aqueous layer was acidified with 1 M aqueous citric acid, and the resulting solid was washed with cold water and dried under vacuum to afford the title compound (2.30 g, 95%) as a white solid. ^{1}H NMR: 1.60 (2H, m), 1.75 (4H, m), 1.88 (3H, m), 2.14 (1H, m), 3.54 (1H, m), 3.71 (1H, q), 3.85 (2H, m), 4.06 (1H, m), 4.40 (1H, m), 7.92 (1H, d), 8.64 (1H, s), 12.42 (1H, s). *m*/*z* MH^+ = 278. HPLC t_R = 1.75 min.

4-Cyclopentyl-*N*-(5-hydroxy-2-adamantyl)-2-[[(3*S*)-oxolan-3-yl]amino]pyrimidine-5-carboxamide (26). HATU (45.1 g, 118.6 mmol) was added to (*S*)-4-cyclopentyl-2-(tetrahydrofuran-3-ylamino)-pyrimidine-5-carboxylic acid (32.9 g, 118.6 mmol) and *i*-Pr_2NEt (41.4 mL, 237.3 mmol) in DMF (300 mL). The resulting solution was stirred at rt for 15 min. *trans*-4-Aminoadamantan-1-ol hydrochloride (29.0 g, 142.4 mmol) was added, and the reaction mixture was stirred at rt overnight, then evaporated, taken up in EtOAc, and washed with water and saturated brine. The organic layer was dried over $MgSO_4$, filtered, and evaporated to afford the crude product, which was purified by FCC, eluting with 0−10% MeOH in EtOAc, then recrystallized from IPA. The resulting solid was suspended in water and heated at reflux for 24 h (to remove residual IPA in crystal lattice), then filtered, and dried under vacuum to afford the title compound (25.8 g, 51%) as a white solid. ^{1}H NMR: 1.29−1.38 (2H, m), 1.54−1.64 (6H, m), 1.65−2.05 (14H, m), 2.09−2.17 (1H, m), 3.38−3.48 (1H, m), 3.50−3.53 (1H, m), 3.67−3.73 (1H, m), 3.81−3.85 (1H, m), 3.86−3.91 (2H, m), 4.30−4.42 (1H, m), 4.38 (1H, s), 7.42−7.54 (1H, m), 8.00−8.07 (1H, m), 8.14 (1H, s). *m*/*z* MH^+ = 427. HPLC t_R = 1.69 min.

See the Supporting Information for the preparation of other representative examples and characterization for all additional examples.

■ ASSOCIATED CONTENT

Supporting Information

Preparation and additional characterization for final compounds, enzymatic assay procedures, procedures and parameters for X-ray crystallography, data set used for Free-Wilson analysis and model coefficients for R1/R2 groups, ex vivo assay and in vivo protocols for PD/efficacy studies, PK/PD parameters for model fitting, and ADMET references. This material is available free of charge via the Internet at http://pubs.acs.org.

Accession Codes

The crystal structure of human 11β-HSD in complex with compounds **3** and **26** has been deposited in the Protein Data Bank (PDB accession codes 4bb6 and 4bb5).

■ AUTHOR INFORMATION

Corresponding Author

*Tel: +44(0)1625 519064. E-mail: frederick.goldberg@astrazeneca.com.

Notes

The authors declare no competing financial interest.

■ ACKNOWLEDGMENTS

We thank Joanne deSchoolmeester for generating high-quality enzyme data, Mark Denn for generation of high-quality PK data, Brendan Leighton for his advice and leadership of the bioscience strategy, Patrik Johansson and Stefan Gerhardt for generation of crystal structures, and Adrian Gill and Martin Wild for their support and leadership of the project.

■ ABBREVIATIONS

c-Pr, cyclopropyl; *c*-Bu, cyclobutyl; *c*-Pn, cyclopentyl; FCC, flash column chromatography; HSD, hydroxysteroid dehydrogenase; HATU, 2-(3H-[1,2,3]triazolo[4,5-b]pyridin-3-yl)-1,1,3,3-tetramethylisouronium hexafluorophosphate(V); HMDS, hexamethyldisilazane; LLE, ligand lipophilicity efficiency (pIC_{50}-$logD_{7.4}$)

■ REFERENCES

(1) Ge, R.; Huang, Y.; Liang, G.; Li, X. 11β-Hydroxysteroid dehydrogenase type 1 inhibitors as promising therapeutic drugs for diabetes: status and development. *Curr. Med. Chem.* **2010**, *17*, 412−422.

(2) Morgan, S. A.; Tomlinson, J. W. 11β-Hydroxysteroid dehydrogenase type 1 inhibitors for the treatment of type 2 diabetes. *Expert Opin. Invest. Drugs* **2010**, *19*, 1067−1076.

(3) Masuzaki, H.; Yasue, S.; Nakao, K. Molecular target of the metabolic syndrome. 11β-HSD1 an adipocyte function. *Card. Pract.* **2005**, *16*, 179−186.

(4) Anagnostis, P.; Athyros, V. G.; Tziomalos, K.; Karagiannis, A.; Mikhailidis, D. P. The pathogenetic role of cortisol in the metabolic syndrome: a hypothesis. *J. Clin. Endocrinol. Metab.* **2009**, *94*, 2692−2701.

(5) Scott, J. S.; Bowker, S. S.; deSchoolmeester, J.; Gerhardt, S.; Hargreaves, D.; Kilgour, E.; Lloyd, A.; Mayers, R. M.; McCoull, W.; Newcombe, N. J.; Ogg, D.; Packer, M. J.; Rees, A.; Revill, J.; Schofield, P.; Selmi, N.; Swales, J. G.; Whittamore, P. R. O. Discovery of a Potent, Selective, and Orally Bioavailable Acidic 11β-Hydroxysteroid Dehydrogenase Type 1 (11β-HSD1) Inhibitor: Discovery of 2-[(3S)-1-[5-(Cyclohexylcarbamoyl)-6-propylsulfanylpyridin-2-yl]-3-piperidyl]acetic Acid (AZD4017). *J. Med. Chem.* **2012**, *55*, 5951−5964.

(6) Scott, J. S.; Gill, A. L.; Godfrey, L.; Groombridge, S. D.; Rees, A.; Revill, J.; Schofield, P.; Sörme, P.; Stocker, A.; Swales, J. G.; Whittamore, P. R. O. Optimisation of Pharmacokinetic Properties in a Neutral Series of 11β-HSD1 Inhibitors. *Bioorg. Med. Chem. Lett.* **2012**, *22*, 6756−6761.

(7) Free, S. M., Jr.; Wilson, J. W. A mathematical contribution to structure-activity studies. *J. Med. Chem.* **1964**, *7*, 395−399.

(8) Freeman-Cook, K. D.; Amor, P.; Bader, S.; Buzon, L. M.; Coffey, S. B.; Corbett, J. W.; Dirico, K. J.; Doran, S. D.; Elliott, R. L.; Esler, W.; Guzman-Perez, A.; Henegar, K. E.; Houser, J. A.; Jones, C. S.; Limberakis, C.; Loomis, K.; McPherson, K.; Murdande, S.; Nelson, K. L.; Phillion, D.; Pierce, B. S.; Song, W.; Sugarman, E.; Tapley, S.; Tu, M.; Zhao, Z. Maximizing lipophilic efficiency: The use of free-wilson analysis in the design of inhibitors of acetyl-CoA carboxylase. *J. Med. Chem.* **2012**, *55*, 935−942.

(9) Patel, Y.; Gillet, V. J.; Howe, T.; Pastor, J.; Oyarzabal, J.; Willett, P. Assessment of Additive/Nonadditive Effects in Structure-Activity Relationships: Implications for Iterative Drug Design. *J. Med. Chem.* **2008**, *51*, 7552−7562.

(10) Thomas, M. P.; Potter, B. V. L. Crystal structures of 11β-hydroxysteroid dehydrogenase type 1 and their use in drug discovery. *Future Med. Chem.* **2011**, *3*, 367−390.

(11) Walker, E. A.; Clark, A. M.; Hewison, M.; Ride, J. P.; Stewart, P. M. Functional Expression, Characterization, and Purification of the Catalytic Domain of Human 11-beta-Hydroxysteroid Dehydrogenase Type 1. *J. Biol. Chem.* **2001**, *276*, 21343−21350.

(12) Maser, E.; Voelker, B.; Friebertshaeuser, J. 11β-Hydroxysteroid Dehydrogenase Type 1 from Human Liver: Dimerization and Enzyme Cooperativity Support Its Postulated Role as Glucocorticoid Reductase. *Biochemistry* **2002**, *41*, 2459−2465.

(13) Hosfield, D. J.; Wu, Y.; Skene, R. J.; Hilgers, M.; Jennings, A.; Snell, G. P.; Aertgeerts, K. Conformational Flexibility in Crystal Structures of Human 11{beta}-Hydroxysteroid Dehydrogenase Type I Provide Insights into Glucocorticoid Interconversion and Enzyme Regulation. *J. Biol. Chem.* **2005**, *280*, 4639−4648.

(14) Favia, A. D.; Masetti, M.; Recanatini, M.; Cavalli, A. Substrate Binding Process and Mechanistic Functioning of Type 1 11β-Hydroxysteroid Dehydrogenase from Enhanced Sampling Methods. *PLoS ONE* **2011**, *6*, e25375.

(15) Zhang, J.; Osslund, T. D.; Plant, M. H.; Clogston, C. L.; Nybo, R. E.; Xiong, F.; Delaney, J. M.; Jordan, S. R. Crystal Structure of Murine 11β-Hydroxysteroid Dehydrogenase 1: An Important Therapeutic Target for Diabetes‡. *Biochemistry (N. Y.)* **2005**, *44*, 6948−6957.

(16) *Maestro*; Schrödinger, LLC: New York, NY, 2011; *9.2*.

(17) Waring, M. J. Lipophilicity in drug discovery. *Expert Opin. Drug Discovery* **2010**, *5*, 235−248.

(18) Waring, M. J. Defining optimum lipophilicity and molecular weight ranges for drug candidates-Molecular weight dependent lower logD limits based on permeability. *Bioorg. Med. Chem. Lett.* **2009**, *19*, 2844−2851.

(19) Kotelevtsev, Y.; Brown, R. W.; Fleming, S.; Kenyon, C.; Edwards, C. R. W.; Seckl, J. R.; Mullins, J. J. Hypertension in mice lacking 11β-hydroxysteroid dehydrogenase type 2. *J. Clin. Invest.* **1999**, *103*, 683−689.

(20) Veniant, M. M.; Hale, C.; Komorowski, R.; Chen, M. M.; St., J., D. J.; Fotsch, C.; Wang, M. Time of the day for 11β-HSD1 inhibition plays a role in improving glucose homeostasis in DIO mice. *Diabetes, Obes. Metab.* **2009**, *11*, 109−117.